UCSF
UC San Francisco Previously Published Works

Title

Androgen Receptor Inhibition Increases MHC Class I Expression and Improves Immune Response in Prostate Cancer

Permalink

https://escholarship.org/uc/item/73k2x1gw

Journal

Cancer Discovery, 15(3)

ISSN

2159-8274

Authors

Chesner, Lisa N
Polesso, Fanny
Graff, Julie N
et al.

Publication Date

2025-03-03

DOI

10.1158/2159-8290.cd-24-0559

Peer reviewed

eScholarship.org Powered by the California Digital Library
University of California

RESEARCH BRIEF

Androgen Receptor Inhibition Increases MHC Class I Expression and Improves Immune Response in Prostate Cancer

Lisa N. Chesner[1,2], Fanny Polesso[3], Julie N. Graff[4,5], Jessica E. Hawley[6,7], Alexis K. Smith[1,2], Arian Lundberg[1,2,18], Rajdeep Das[1,2], Tanushree Shenoy[1,8], Martin Sjöström[1,2], Faming Zhao[9], Ya-Mei Hu[9], Simon Linder[10], William S. Chen[1,2], Reed M. Hawkins[3], Raunak Shrestha[1,2], Xiaolin Zhu[1,8], Adam Foye[1,8], Haolong Li[1,2], Lisa M. Kim[1,2], Megha Bhalla[1,2], Thomas O'loughlin[1,11], Duygu Kuzuoglu-Ozturk[1,11], Junjie T. Hua[1,2], Michelle L. Badura[1,2], Scott Wilkinson[12], Shana Y. Trostel[12], Andries M. Bergman[10], Davide Ruggero[1,11,13], Charles G. Drake[14,15], Adam G. Sowalsky[12], Lawrence Fong[1,6,7,8], Matthew R. Cooperberg[1,11,16], Wilbert Zwart[10], Xiangnan Guan[9], Alan Ashworth[1,8], Zheng Xia[4,9,17], David A. Quigley[1,11,16], Luke A. Gilbert[1,11], Felix Y. Feng[1,2,8,11], and Amy E. Moran[3,4]

ABSTRACT

Tumors escape immune detection and elimination through a variety of mechanisms. Here, we used prostate cancer as a model to examine how androgen-dependent tumors undergo immune evasion through downregulation of the major histocompatibility complex class I (MHCI). We report that response to immunotherapy in late-stage prostate cancer is associated with elevated MHC expression. To uncover the mechanism, we performed a genome-wide CRISPR interference (CRISPRi) screen and identified androgen receptor (*AR*) as a repressor of the MHCI pathway. Syngeneic mouse models of aggressive prostate cancer deficient in *Ar* also demonstrated increased tumor immunogenicity and promoted T cell–mediated tumor control. Notably, the increase in MHCI expression upon AR blockade is transient and correlates with resistance to AR inhibition. Mechanistic studies identified androgen response elements upstream of MHCI transcription start sites which increased MHCI expression when deleted. Together, this body of work highlights another mechanism by which hormones can promote immune escape.

SIGNIFICANCE: Immunotherapy options for immune cold tumors, like prostate cancer, are limited. We show that AR downregulates MHCI expression/antigen presentation and that AR inhibition improves T-cell responses and tumor control. This suggests that treatments combining AR inhibitors and checkpoint blockade may improve tumor immune surveillance and antitumor immunity in patients.

[1]Helen Diller Family Comprehensive Cancer Center, University of California, San Francisco, San Francisco, California. [2]Department of Radiation Oncology, University of California, San Francisco, San Francisco, California. [3]Department of Cell, Developmental and Cancer Biology, Oregon Health and Science University, Portland, Oregon. [4]Knight Cancer Institute, Oregon Health and Science University, Portland, Oregon. [5]VA Portland Health Care System, Portland, Oregon. [6]Department of Medicine, University of Washington, Seattle, Washington. [7]Clinical Research Division, Fred Hutch Cancer Center, Seattle, Washington. [8]Divsion of Hematology and Oncology, Department of Medicine, University of California, San Francisco, San Francisco, California. [9]Department of Biomedical Engineering, Oregon Health & Science University, Portland, Oregon. [10]Division of Oncogenomics, Oncode Institute, The Netherlands Cancer Institute, Amsterdam, the Netherlands. [11]Department of Urology, University of California San Francisco, San Francisco, California. [12]Genitourinary Malignancies Branch, National Cancer Institute, Bethesda, Maryland. [13]Department of Cellular and Molecular Pharmacology, University of California, San Francisco, San Francisco, California. [14]Department of Medicine, Herbert Irving Comprehensive Cancer Center, Columbia University, New York, New York. [15]Department of Urology, Herbert Irving Comprehensive Cancer Center, Columbia University, New York, New York. [16]Department of Epidemiology and Biostatistics, University of California, San Francisco, San Francisco, California. [17]Center for Biomedical Data Science, Oregon Health & Science University, Portland, Oregon. [18]Department of Protein Science, SciLifeLab, KTH Royal Institute of Technology, Stockholm, Sweden.

F.Y. Feng and A.E. Moran contributed equally to this article.

Current address for R. Das, University Hospitals Cleveland Medical Center and Case Western Reserve University School of Medicine, Cleveland, Ohio; and current address for C.G. Drake, Janssen R&D, Spring House, Pennsylvania.

Corresponding Authors: Amy E. Moran, Department of Cell, Developmental and Cancer Biology, Oregon Health and Science University, Knight Cancer Research Building, Room 3006, 2720 S Moody Avenue, Portland, OR 97201. E-mail: moranam@ohsu.edu; and Felix Y. Feng, Department of Radiation Oncology, University of California, San Francisco, Box 3110, Room 450, 1450 3rd Street, San Francisco, CA 94158. E-mail: Felix.Feng@ucsf.edu

Cancer Discov 2025;15:481–94

doi: 10.1158/2159-8290.CD-24-0559

This open access article is distributed under the Creative Commons Attribution-NonCommercial-NoDerivatives 4.0 International (CC BY-NC-ND 4.0) license.

©2024 The Authors; Published by the American Association for Cancer Research

INTRODUCTION

A fundamental component of antitumor immunity is the expression of the major histocompatibility complex class I (MHCI) on tumor cells. In the past decade, mechanisms of immune escape via loss of MHCI have been described (1–6). Furthermore, resistance to immune checkpoint blockade (ICB) is associated with loss of MHCI (5). Given this, efforts have been invested toward understanding the mechanisms of immunotherapy resistance. Some seem to be shared between tumor types (i.e., PD-1+ lymphocytes) and others unique to the tissue of origin (6–8). It is plausible that just as viruses utilize distinct immune evasion tactics based on tissue tropism, cancer cells might have mechanisms of immune evasion that reflect unique attributes of their tissue microenvironment and/or oncogene addiction. In this regard, prostate cancer represents an appropriate disease for investigating the crosstalk between androgens and tumor immune evasion.

Prostate cancer, as compared with lung cancer, has a low response rate to ICB and markedly lower MHCI expression (Fig. 1A; refs. 1, 9, 10). The molecular mechanisms that control MHCI expression in prostate cancer remain unknown despite evidence that androgen deprivation therapy (ADT) is initially immunogenic, recruiting leukocytes into the tissue (11, 12). In a clinical trial designed to investigate the early effects of ADT on the prostate tumor landscape, there was an initial infiltration of mononuclear cells that corresponded to increased cell death (13). By week 4 after ADT initiation, tumor cell death plateaued, as did the infiltration of mononuclear cells. Despite evidence of ADT-induced immunogenicity, prostate cancer immunotherapy trials are repeatedly negative. Therefore, there is a critical need to understand the mechanisms of immunotherapy resistance in this disease.

In this study, we employed a genome-wide CRISPR interference (CRISPRi) flow cytometry-based screen to identify the regulators of MHCI in prostate cancer cells. Significant hits involved in androgen receptor (*AR*) signaling were validated as suppressors of MHCI using *in vitro* and *in vivo* models as well as observed in four phase II clinical trials. Interestingly, the top regulators of MHCI in prostate cancer were distinct from those recently identified in a similar immune evasion CRISPR screen in AML (2) or reported in melanoma (4–6). Thus, these screens undoubtedly help identify disease-specific regulators of immune evasion to inform tumor-specific combination therapies and improve ICB efficacy in MHC-low tumors, such as prostate cancer.

RESULTS

AR Represses MHCI in Prostate Cancer

We previously reported that one mechanism of ICB resistance in advanced prostate cancer is through AR suppression of CD8 T-cell function (14). Using the same dataset, we observed an increased MHCI expression in ICB responders (Fig. 1B). To explore MHCI regulation in prostate cancer, we conducted a genome-wide CRISPRi screen using a metastatic castration-resistant prostate cancer (mCRPC) line, C42B, stably expressing a non-catalytic Cas9 (dCas9-KRAB fusion protein). Cells were infected (15), selected, and sorted based on highest and lowest (25%–30%) MHCI expression (Fig. 1C). Gene hits were ranked by phenotype score (Fig. 1D; Supplementary Table S1). As expected, gene hits in the MHCI processing pathway (*B2M*, *TAP1*, *HLA-A*, *TAPBP*, *TAP2*, and *IRF2*) decreased MHCI expression upon knockdown. Interestingly, suppression of *AR* increased MHCI expression. AR coregulators (16, 17), *GRHL2* and *FOXA1*, were also shown to significantly increase MHCI expression upon knockdown. We validated these findings by knocking down *AR*, *GRHL2*, *FOXA1*, and *B2M* using individual sgRNAs and compared MHCI expression to control (*GAL4*) in C42B and LNCaP cells (Fig. 1E; Supplementary S1A and S1B). These results revealed increased MHCI expression upon knockdown of *AR* and AR signaling genes. Further, knocking down AR genes improved MHCI upregulation in response to interferon gamma (IFNγ) treatment (Supplementary Fig. S1C and S1D). Overexpressed *AR* in the AR-null PC3 prostate cancer cell line demonstrated decreased MHCI processing and presentation genes and expression in *AR*-positive PC3 cells compared with *AR*-null cells (Fig. 1F–H).

Pharmacologic Inhibition of AR Modulates MHCI

sgRNA gene targeting has variable knockdown efficiency (Supplementary Fig. S1E and S1F); thus, we treated C42B cells with various AR inhibitors and observed increasing MHCI over time (Fig. 2A). Expression of MHCI-associated genes/protein could be repressed by the exogenous AR ligand R1881 (Fig. 2B; Supplementary Fig. S2A and S2B). Additional prostate cancer models with various *AR* expression levels (C42B, LNCaP, VCaP, PC3) were treated with enzalutamide (Fig. 2C–F), the AR degrader (ARD; Supplementary Fig. S2C–S2F; refs. 18, 19), or CSS (Supplementary Fig. S2G–S2J) and also demonstrated increased expression of MHCI and antigen presentation genes. Given AR inhibition is reported to induce type I interferons (20, 21), we evaluated interferon response genes following enzalutamide treatment and observed an increase in a few genes (Supplementary Fig. S2K).

Notably, we observed a rapid drop of MHCI within a week after removing AR inhibition, which returned to baseline by 2 weeks (Fig. 2G), suggesting active AR inhibition is required to maintain MHCI. To determine the stability of elevated MHCI with AR inhibition, C42B cells were treated with enzalutamide and MHCI expression measured over 3 months revealing two phases of sensitivity to androgen blockade and MHCI expression. In the first 30 days, MHCI expression was significantly increased, corresponding with growth arrest (Fig. 2H), followed by loss of expression and tumor cell growth. Curious if this was associated with AR reactivation, we evaluated the mRNA expression via RNA sequencing (RNA-seq) at 28, 49, and 91 days posttreatment (Fig. 2I; Supplementary Tables S2A–S2C). Interestingly, loss of MHCI is proceeded by an increase in *NR3C1*, the glucocorticoid receptor (Fig. 2J).

AR Transcriptionally Represses MHCI Gene Expression

To determine if AR regulated MHCI through binding to androgen response elements (ARE), we identified AREs within 10 kb of MHCI transcriptional start sites (TSS) and designed sgRNAs to target these sites using Cas9 nuclease (Supplementary Table S3). We conducted a lentiviral pooled CRISPR

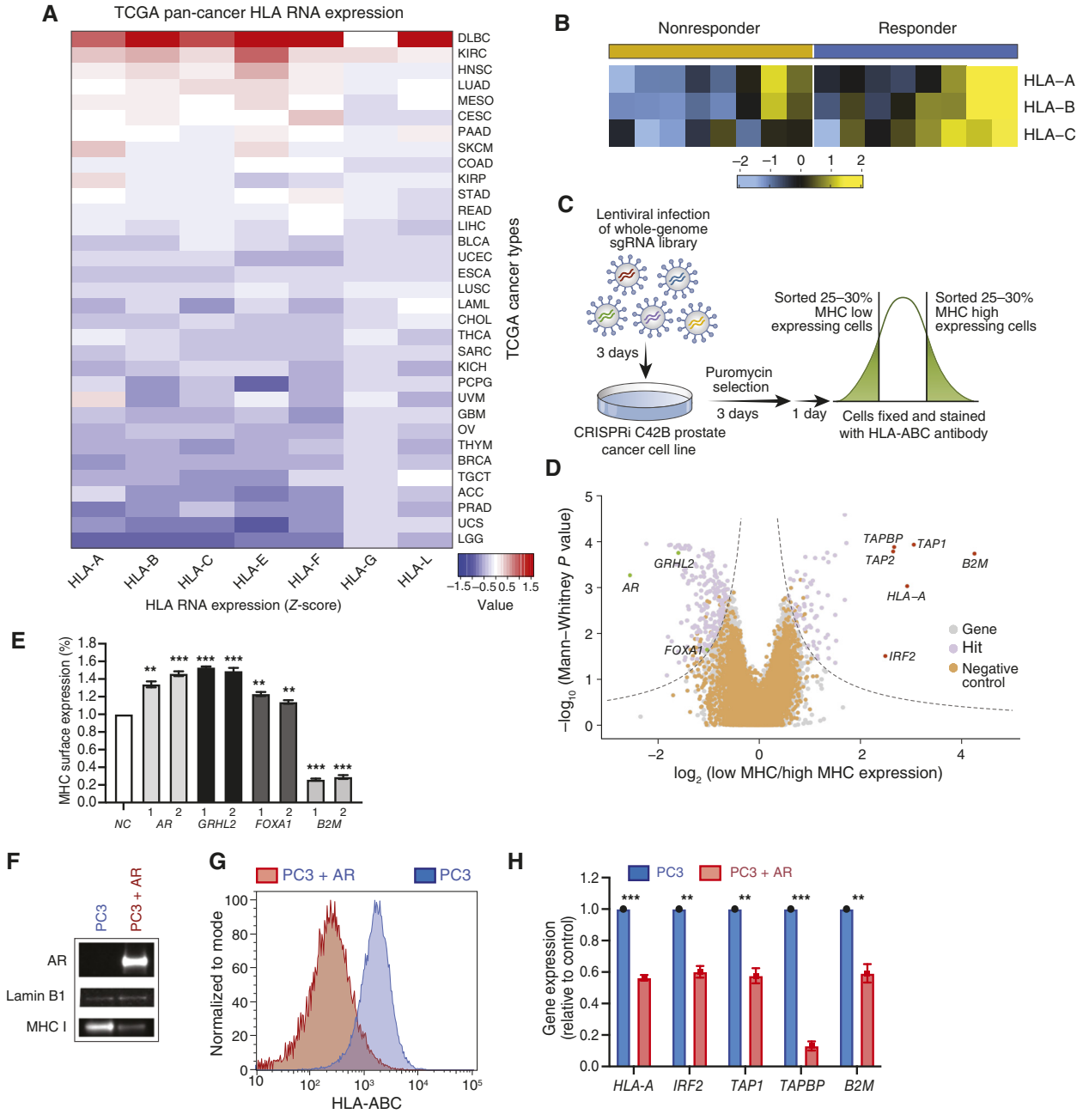

Figure 1. *AR* represses MHCI in prostate cancer. **A,** Heatmap of median RNA expression of HLA genes in the TCGA Pan Cancer cohort. **B,** Heatmap of scaled RNA expression of MHC genes in nonresponders and responders to pembrolizumab treatment of patients with mCRPC. **C,** Schematic of a genome-wide CRISPRi screen based on surface expression of MHCI in C42B-dCas9 prostate cancer cells. **D,** Volcano plot showing Mann–Whitney statistical significance and average phenotype score of gene hits (purple) and negative controls (orange). **E,** MHCI expression of C42B-dCas9 cells infected with sgRNAs targeting *GAL4* (control), *AR*, *GRHL2*, *FOXA1*, or *B2M* ($n = 3$ as biological replicates; mean ± SEM). **F–H,** MHCI expression assessed using Western blot (**F**), flow cytometry (**G**), or qRT-PCR (**H**) of *AR*-null or *AR*-positive PC3 cells. ** p<0.01, *** p<0.001.

screen targeting 41 AREs, as well as *AR*, *GRHL2*, and *FOXA1* (positive controls) and *B2M*, *HLA-A*, and *TAP* genes (negative controls; Fig. 2K). The screen confirmed that *AR*, *FOXA1*, and *GRHL2* inhibition increased MHCI expression and knockout of *B2M*, *TAP*, and *HLA-A* decreased MHCI expression (Fig. 2L). ARE motifs in *NLRC5*, *CANX*, *TAP2*, *TAP1*, and *IRF2* were individually targeted using sgRNAs, single-cell cloned, and confirmed on-target cutting efficiency. ARE-deleted clones showed increased MHCI expression by flow cytometry (Fig. 2M) and qRT-PCR (Fig. 2N). We also utilized publicly available ChIP-seq data (22) to query AREs targeted in our CRISPR screen and found decreased *AR* binding (Fig. 2O; Supplementary Fig. S3A and S3B) and increased H3K27ac (Supplementary Fig. S3C and S3D) after enzalutamide treatment.

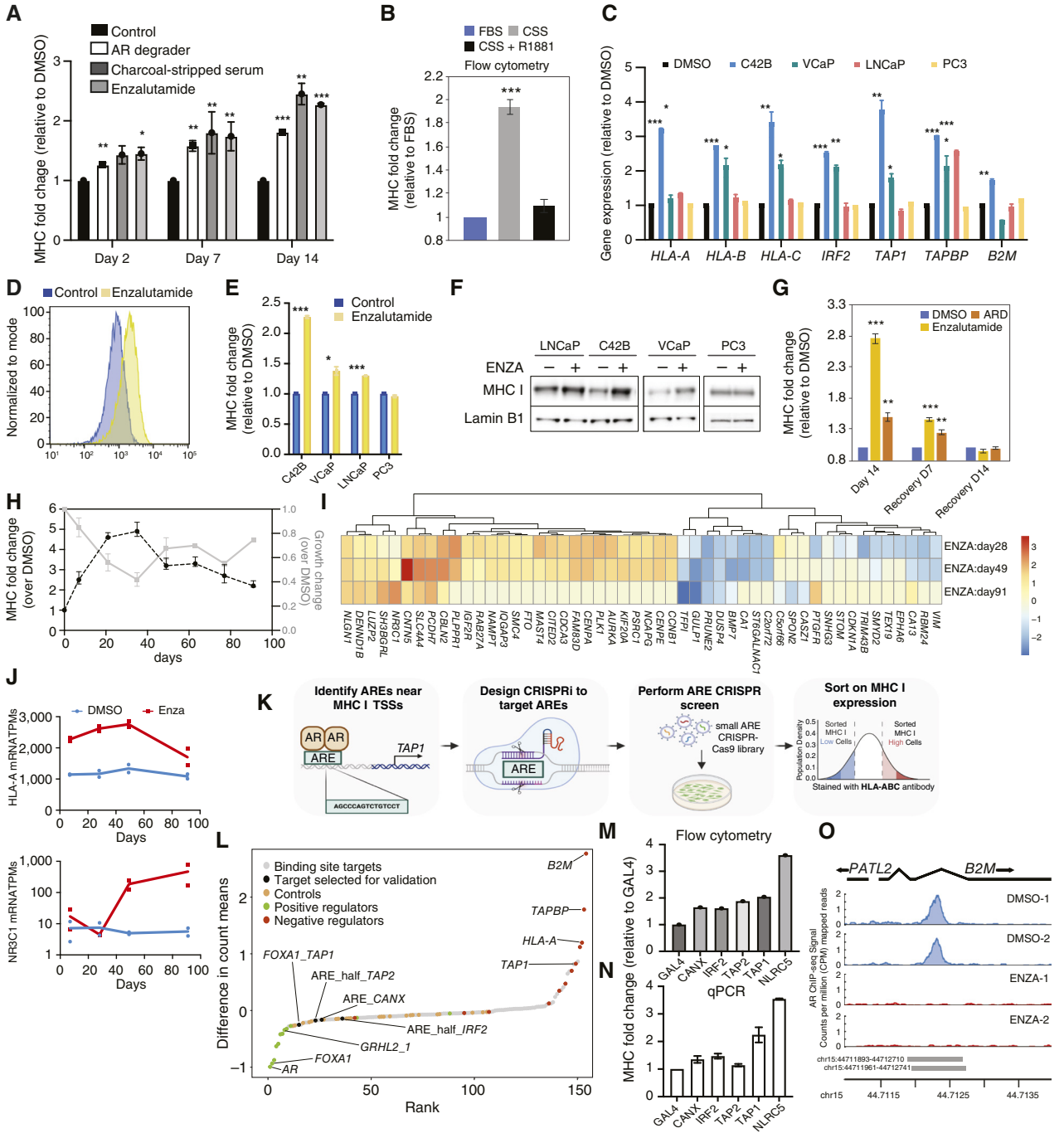

Figure 2. *AR* transcriptionally represses MHCI expression. **A,** MHCI expression of C42B cells treated with ARD-61, CSS, or enzalutamide for 2, 7, or 14 days ($n = 3$ as biological replicates; mean ± SEM). **B,** MHCI expression of C42B cells treated with CSS for 14 days with or without R1881 ($n = 3$ as biological replicates; mean ± SEM). **C–F,** C42B, VCaP, LNCaP, and PC3 cells treated with enzalutamide for 14 days. **C,** Gene expression of MHCI processing genes ($n = 3$ as biological replicates; mean ± SEM), (**D**) C42B cells stained with an HLA-ABC antibody, (**E**) MFI of cells stained with an HLA-ABC antibody ($n = 3$ as biological replicates; mean ± SEM), and (**F**) MHCI protein levels. **G,** MHCI expression of C42B cells treated with either ARD-61 or enzalutamide for 14 days after which the drug was removed and MHC expression assessed 7 or 14 days later ($n = 3$ as biological replicates; mean ± SEM). **H,** C42B cells treated with DMSO or enzalutamide for 91 days. Black: MFI fold change after staining with an HLA-ABC antibody. Gray: Change in growth compared with DMSO-treated cells ($n = 3$ as biological replicates; mean ± SEM). **I,** Heatmap of effect size on mRNA expression after enzalutamide treatment in C42B cells for the top 50 most significant genes evaluated for treatment × time interaction. **J,** mRNA of *HLA-A* and *NR3C1* (in length-scaled TPM) over time. **K,** Schematic of a CRISPR screen targeting AREs near MHCI TSSs (Created in BioRender. Chesner, L. (2024) BioRender.com/r09b289). **L,** Differences in means of gene hits ranked from a CRISPR screen targeting AR and FOXA1 binding sites near MHCI genes. **M,** MHCI expression of C42B ARE-deficient clones near *CANX*, *IRF2*, *TAP2*, *TAP1*, or *NLRC5*. **N,** Gene expression of *CANX*, *IRF2*, *TAP2*, *TAP1*, or *NLRC5* in ARE-deficient clones compared with *GAL4*. **O,** AR ChIP-seq peak signal around an ARE near the *B2M* promoter (*P* value = 0.001) after DMSO (blue) or enzalutamide treatment (red). Horizontal bars at the bottom indicate ARE. * p<0.05, ** p<0.01, *** p<0.001.

Finally, we treated two control (GAL4) or ARE-deleted (CANX) clones with enzalutamide and assessed MHCI expression after 7 days (Supplementary Fig. S3E–S3G). These experiments showed a larger increase in MHCI expression in the control than in the ARE-deleted clones (Supplementary Fig. S3H), suggesting that the deletion of AREs prevents the transcriptional repression of MHCI genes.

AR Inhibition Increases T-cell Cytotoxicity

To see if increasing MHCI expression by AR inhibition could improve antitumor T-cell responses, we transfected human CD8 T cells with an *HLA-A2*-restricted TCR specific for the cancer testis antigen *NY-ESO1* (Supplementary Fig. S4A). *HLA-A2*-restricted *NY-ESO1*-expressing C42B cells (Fig. 3A) were treated with AR inhibitors, washed, replated, and cocultured with *NY-ESO1*-reactive CD8 T cells. These experiments showed increased T-cell cytotoxicity and a reduction in tumors pretreated with an AR inhibitor compared with control (Fig. 3B and C; Supplementary Fig. S4B–S4E), an observation that was dependent upon MHCI expression on the tumor cells (Fig. 3D; Supplementary Fig. S4D). C42B cells that did not express *NY-ESO1* and cocultured with T cells were not killed when treated with AR inhibitors (Supplementary Fig. S4F), demonstrating that AR inhibition enhances T-cell recognition of target cells in an MHCI-dependent manner.

Tumor Cell-Intrinsic AR Knockdown Increases CD8 T cell–Mediated Antitumor Immunity

To explore our observation *in vivo*, the TrampC1 tumor model, which has a known MHCI-restricted tumor antigen, stimulator of prostatic adenocarcinoma (*Spas-1*; ref. 23), and low expression of MHCI, and the PPSM (*Pten*−/−; *p53*−/−; *Smad4*−/−) model, which is androgen insensitive, were employed (24). We knocked down *Ar* (*Ar*-KD; Supplementary Fig. S5A and S5B), generated single-cell clones, and observed comparable growth *in vitro* to wild-type (WT) cells (Supplementary Fig. S5C and S5D). Loss of *Ar* in TrampC1 cells increased MHCI expression (Fig. 3E) and sensitivity to IFNγ-induced MHCI expression (Fig. 3F). *In vivo* (Fig. 3G), TrampC1 *Ar*-KD tumors were significantly smaller (Fig. 3H), and the number of tumor-infiltrating CD8 T cells was significantly greater in *Ar*-KD tumors (Fig. 3I). Using the *Nur77*GFP mouse in which GFP is upregulated by TCR engagement (25) and can be used as a tool to identify tumor-reactive T cells that recently received strong TCR signals (26), we observed significantly increased *Nur77*GFP^{hi} CD8 T cells in *Ar*-KD tumors (Fig. 3J). Furthermore, we recovered more *Spas1* tetramer-positive CD8 T cells in *Ar*-KD tumors (Fig. 3K and L; Supplementary Fig. S5E) and upon stimulation observed a significant increase in the total number of IFNγ-producing CD8 T cells in *Ar*-KD tumors compared with WT (Fig. 3M and N). Finally, we explored the requirement for T cell–mediated tumor control in our models. In the absence of lymphocytes (*Rag*-KO), we observed no difference in tumor growth in *Ar*-KD versus WT (Fig. 3O and P) and extended these observations into the PPSM model (Supplementary Fig. S5F–S5H). Overall, our data suggest that loss of tumor-intrinsic *Ar* expression increases MHCI expression and the frequency and function of tumor-specific CD8 T cells, enhancing tumor control.

MHCI Expression Increases following *AR* Inhibition in Patients with Prostate Cancer

Last, we explored evidence for androgen axis-targeted therapies modulating MHCI in patients. We analyzed RNA expression data from a phase 2 clinical trial that studied the effects of enzalutamide in early prostate cancer (NCT03297385; ref. 27). Paired biopsies from treatment-naïve patients and 3 months after neoadjuvant enzalutamide treatment without ADT showed significantly increased transcription of *HLA-A* and *B2M* and MHC-regulating genes *IRF1* and *IRF2* posttreatment (Fig. 4A) and an enrichment of interferon activity (Supplementary Fig. S6A). These data were consistent with data from a second cohort of patients (NCT02430480) treated for 6 months with neoadjuvant ADT plus enzalutamide (Fig. 4B; Supplementary Fig. S6B; ref. 28). Pathway analysis of these paired biopsies also revealed an increase in antigen presentation (Supplementary Tables S4 and S5). To determine if this correlation was observed in lethal, metastatic castration-resistant disease, we generated an MHCI signature (see "Methods"), applied it to a hormone-refractory metastatic prostate cancer biopsy dataset (29), and observed a significant negative correlation between MHCI activity and *AR* activity (Fig. 4C).

To determine if there was clinical significance to our observations in the context of immunotherapy, we leveraged a single-cell dataset in metastatic hormone-sensitive prostate cancer (mHSPC; ref. 30). Two groups of patients permitted analysis of tumor cell-intrinsic changes in MHCI with ADT (on ADT) versus ADT with anti-PD1 (on combination). Cells from all patients were combined and clustered into hematopoietic and non-hematopoietic cells (Fig. 4D; Supplementary Fig. S6C). There was a distinct luminal epithelia cell cluster (EPCAM+AR+TMPRSS2+, Supplementary Fig. S6C), which we evaluated for pretreatment *AR* and MHCI gene expression. Pretreatment lesions had low MHCI processing and presentation gene expression and high *AR* and *AR* target genes (Fig. 4E). Using the Virtual Inference of Protein-activity by Enriched Regulon analysis (VIPER) to infer protein activity (31), we observe decreased *AR* activity and a corresponding increase in MHCI activity with treatment (Supplementary Fig. S6D and S6E). Isolating only epithelial cells, we observed a clear conserved reduction of *AR* activity in paired individual biopsies in both treatment groups with a strong increase in MHCI with ADT that was further increased with ADT+anti-PD1 (Fig. 4F and G). The increased MHCI with anti-PD1 treatment likely reflects an increase in T-cell-derived IFNγ activity (14) that was not observed with ADT alone but was significantly increased with ADT+anti-PD1 (Supplementary Fig. S6F and S6G).

DISCUSSION

Immunotherapy has become a mainstay of the oncology landscape for many solid tumors. In prostate cancer, the low response rate to immunotherapy has been seen as a failure of the treatment to restore T-cell function. However, an alternative hypothesis is plausible; failure of immunotherapy responses in patients with prostate cancer reflects our

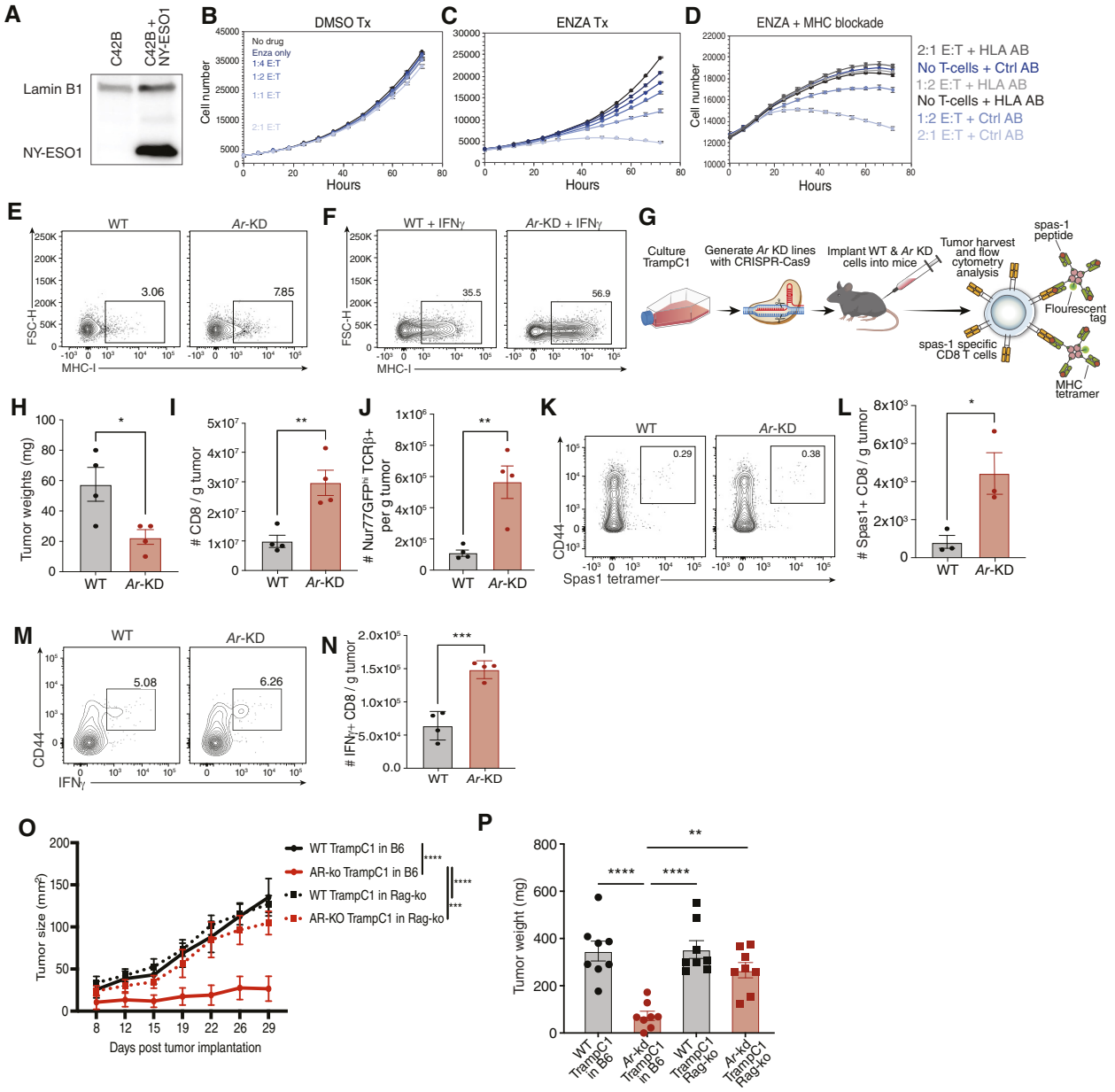

Figure 3. *AR* inhibition increases T-cell cytotoxicity *in vitro* and *in vivo*. **A,** Expression of *NY-ESO1* in C42B cells. **B** and **C,** *NY-ESO1*-expressing C42B cells treated with either DMSO (**C**) or enzalutamide (**D**) for 14 days and then cocultured with CD8 T cells transduced with a *NY-ESO1* TCR for 3 days. **D,** *NY-ESO1*-expressing C42B cells treated with enzalutamide for 14 days and then cocultured with CD8 T cells transduced with a *NY-ESO1* TCR for 3 days in the presence of an HLA-blocking antibody or control antibody. **E** and **F,** MHCI expression of WT or *Ar*-KD TrampC1 cells without (**E**) or with (**F**) rIFNγ treatment. **G,** Schematic of *in vivo* TrampC1 tumor experiment. **H,** Tumor weights at time of harvest (day 12 posttumor implantation). **I,** Number of CD8 T cells in WT or *Ar*-KD TrampC1 tumors. **J,** Number of *Nur77*-GFP+ T cells in WT or *Ar*-KD TrampC1 tumors. **K,** Representative cytograms showing CD44 and *Spas1* tetramer staining in the tumor. Gated on live, TCRβ+, CD8+. **L,** Number of *Spas1* tetramer + CD8 T cells in the tumor. **M,** Representative cytograms showing CD44 and IFNγ expression in CD8 T cells in the tumor. Gated on live, TCRβ+, CD8+. **N,** Number of IFNγ-expressing CD8 T cells in the tumor. **O,** Growth curves of WT and *Ar*-KD TrampC1 tumors in WT and *Rag*-KO animals. **P,** Tumor weights on day 29. Data representative of two to four independent experiments, with three to four animals per group for **D–J** and eight animals per group for **K** and **L**. For **D–F**, **H**, and **J**, unpaired two-tailed Student *t* test. For **K** and **L**, Two-way ANOVA, *, $P < 0.05$; **, $P < 0.01$; ***, $P < 0.001$; ****, $P < 0.0001$.

limited understanding of what regulates immunity in this tissue microenvironment. In this regard, we set out to identify regulators of MHCI in prostate cancer with the goal of understanding the mechanisms of response and resistance in this disease. Importantly, our investigation herein compliments a previous report that *AR* inhibition leads to aberrant endogenous retrovirus regulation, thereby inducing type I interferons and MHCI (21), a mechanism that is likely synergistic with the work presented here.

The interaction between hormones and immune responses is extremely complex with cell-intrinsic and cell-extrinsic mechanisms at play. There is growing evidence that the sexual

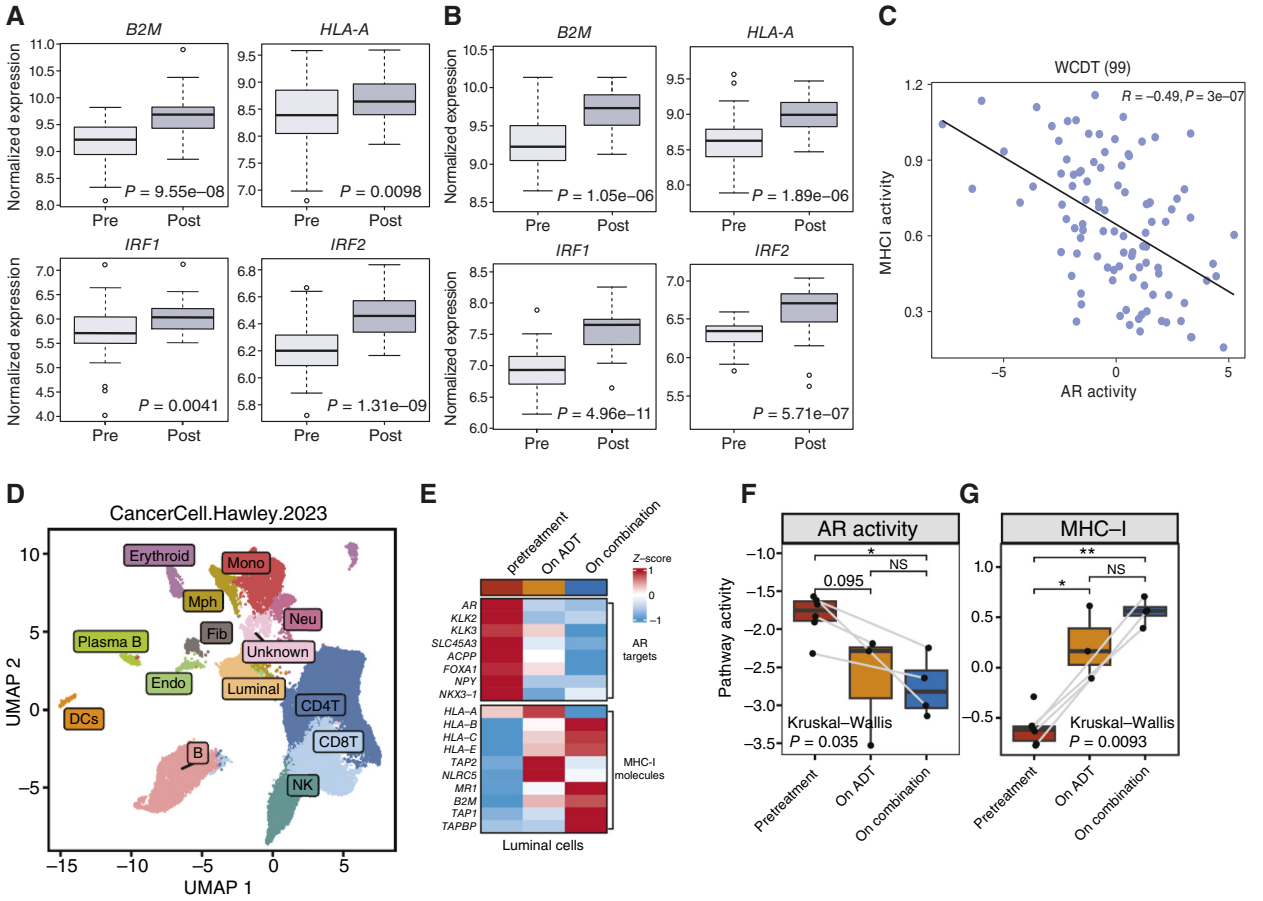

Figure 4. MHCI expression increases following AR inhibition in patients with prostate cancer. **A,** Bulk RNA expression of MHCI-related genes from primary prostate cancer tissues before and after 3 months of neoadjuvant enzalutamide treatment without ADT. **B,** Bulk RNA expression of MHCI-related genes from paired prostate tissues pre- and posttreatment with 6 months neoadjuvant ADT plus enzalutamide. **C,** Scatterplot showing the correlation between AR activity and MHCI activity in WCDT cohort ($n = 99$). Statistical significance was evaluated using two-tailed Pearson's correlation test. **D,** UMAP showing the distribution of 14 major cell types from human PCa scRNA-seq dataset (30). DCs, dendritic cells; Endo, endothelial cells; Fib, fibroblasts; Mono, monocytes; Mph, macrophages; Neu, neutrophils. +ADT = 4 weeks after ADT, +ADT + anti-PD1 = 10 weeks after ADT+anti-PD1 and/or upon recurrence. **E,** Heatmap illustrating expression (Z-score normalization) of genes associated with indicated pathways within luminal cells among different treatment groups. On combination, ADT+anti-PD1 treatment group. **F** and **G,** Box plots showing the activity of *AR* (**F**) or MHCI (**G**) pathways within luminal cells among treatment groups from the PCa scRNA-seq dataset. Each dot represents an individual sample of PCa. Paired patient analysis (indicated by gray line); NS, not significant ($P \geq 0.05$); *, $P < 0.05$; **, $P < 0.01$.

dimorphism observed in inflammatory diseases, such as cancer, is in part mediated by androgen signaling (32–36). In a recent study of individuals receiving gender-affirming hormone therapy, testosterone treatment repressed antigen presentation pathways in circulating monocytes (37). In another study, 17 different mouse tissues were profiled to reveal sex differences mediated by androgens, and of the top 10 genes differentially expressed in male and female mice, 9 were MHCI genes (38). Together, these recent bodies of work highlight the immunomodulatory nature of androgens but come up short in providing a mechanism. Herein, we provide a mechanistic link via *AR* which directly represses MHCI expression (Supplementary Fig. S7). Interestingly, in a phase I clinical trial in men with nivolumab-refractory melanoma, patients were treated for 28 days with an *AR* axis inhibitor in an effort to make them sensitive to immunotherapy. A RECIST of 42.8% was reported in this small study (39), suggesting the potential clinical application of androgen axis inhibition in improving immunotherapy responses in other tumors that have hijacked androgen signaling to evade immunity.

Our investigation of AR regulation of MHCI expression also revealed a temporal period in which androgen axis blockade was immunostimulatory. Over 91 days, early androgen axis inhibition was immunomodulatory and corresponded with tumor cell growth arrest. As the tumor cells transitioned from a period of arrest to growth, MHCI expression also decayed. Notably, under chronic AR inhibition, tumor cells increased *GR* expression prior to loss of MHCI, suggesting a possible transition of AR- to GR-mediated repression of MHCI (40). GR-conferred repression of MHCI upon chronic *AR* inhibition is perhaps not surprising as this has been reported for tumor cell survival in other prostate cancer models (41). Unique to our discovery is the idea that perhaps GR promotes immune evasion in addition to cell survival.

Finally, our observation of a potential AR-to-GR switch is interesting considering the design of immunotherapy clinical trials in prostate cancer and standard of care treatment for this patient population. The KEYNOTE 991 trial (35) was the largest clinical study to date that tested the hypothesis that early combination of androgen axis inhibition with immunotherapy in patients with mHSPC would be effective. Unfortunately, the trial was ended due to a lack of signal in combination therapy over the control arm. The trial was designed to enroll patients with no prior history of androgen axis blockade; however, patients were allowed to be treated for up to 3 months with ADT prior to starting immunotherapy. Given the work of others, as well as data presented herein, androgen axis blockade might be initially immunogenic but then lost due to the activation of other nuclear receptors that repress MHCI. Future immunotherapy clinical trials should be designed to harness the window of ADT-induced immunogenicity and/or the development of biomarkers to identify patients for which androgen axis blockade remains immunogenic.

METHODS

Cell Lines and Reagents

Most cell lines were originally purchased from the ATCC and cultured following standard ATCC protocols. C42B-dCas9 and LNCaP-dCas9 cell lines [generated by Das and colleagues (RRID:CVCL_0395; ref. 42)] and TrampC1 cells were cultured in RPMI 1640 medium (Gibco) with 10% (Gibco) and 5% penicillin/streptomycin (Invitrogen). VCaP (RRID:CVCL_2235), PC3 (RRID:CVCL_0035), and HEK293T cells (RRID:CVCL_0063) were cultured in DMEM (Gibco) with 10% FBS and 5% penicillin/streptomycin. For *AR*-positive PC3 cells, a lentiviral vector was designed to express *AR*-ORF and mCherry selection marker in PC3 cells. HEK293T cells were transfected with *AR*/mCherry-expressing lentiviral plasmid together with a second-generation psPAX2 (RRID:Addgene_12260) packaging vector and pMD2.G (RRID:Addgene_12259) envelope-expressing plasmid. The virus was harvested 24 and 48 hours post-transfection and precipitated using Lenti-X concentrator (Takara). PC3 cells were transduced with virus in the presence of polybrene (4 μg/mL) for 24 hours, and mCherry-positive cells were sorted using Aria (BD). All cells were grown in a 5% CO_2 humidified incubator at 37°C. Cell line STR authentications were done at the UC Berkeley DNA Sequencing Facility. Mouse *Pten*$^{-/-}$; *p53*$^{-/-}$; *Smad4*$^{-/-}$ (PPSM) castration-resistant prostate tumor model was a gift from R. DePinho. TrampC1 cells were purchased from ATCC (RRID:CVCL_3614). Cell lines were STR authenticated prior to use, tested for mycoplasma monthly, and used under passage 50. Enzalutamide was purchased from Selleckchem, and the AR PROTAC degrader ARD-61 was a gift from Dr. Shaomeng Wang's lab at the University of Michigan (18).

CRISPRi Flow Cytometry Screen

The genome-wide CRISPRi flow cytometry screen was performed using the Weissman lab protocol (weissmanlab.ucsf.edu) with some modifications (43). In brief, C42B-dCas9 cells were generated by infecting C42B cells with a lentivirus containing dCas9-KRAB (KRAB domain, Krüppel-associated box), a repressive chromatin-modifying complex to induce transcriptional silencing. dCas9 (from *Streptococcus pyogenes*) was fused to two copies of a nuclear localization signal, HA tag, and blue fluorescent protein (44). Approximately 132 million C42B-dCas9 cells were then infected in duplicate with a lentivirus containing the CRISPRi-V2 library (RRID:Addgene_1000000093), a kind gift from Dr. Luke Gilbert's lab at UCSF, at an MOI of 0.3 and 8 μg/mL polybrene (TR-1003-G). After 3 days, cells were put into media containing 8 μg/mL puromycin (A11138-03). After another 3 days, cells were placed into drug-free media and allowed to recover for 24 hours. Cells were then harvested and fixed in 4% PFA (5 million cells per 1 mL of PFA solution) at room temperature for 20 minutes, washed with cold 1× PBS, and incubated with human Fc Block (564220) in FACS buffer for 10 minutes at room temperature. An anti-human HLA-ABC antibody was then added (Thermo Fisher Scientific, Cat# 17-9983-42, RRID:AB_10733389) and incubated on ice for 20 minutes in the dark. Finally, cells were washed and resuspended in cold FACS buffer and sorted on a BD FACSAria Fusion cell sorter to collect the 25% to 30% highest and lowest HLA-ABC-expressing cells. This protocol was also followed for the ARE sub-library CRISPR screen in C42B cells, using virus generated as described below. DNA was extracted using the Zymo Quick-DNA FFPE Kit (56404) and amplified for 26 cycles using NEBNext Ultra II Q5 Master Mix (M0544S) and primers containing TruSeq indexes for NGS analysis. Libraries were gel purified and extracted using the Zymoclean Gel DNA Recovery Kit (11-301C) and assessed on a high-sensitivity DNA bioanalyzer kit (5067-4626). Sample libraries were run on a HiSeq 4000 and analyzed using standard protocols (ScreenProcessing) as previously described (43).

Lentivirus Generation and Infection

To validate gene hits from the CRISPRi flow cytometry screen, sgRNA sequences (Supplementary Table S6) were cloned into the pLG20 pU6-sgRNA Ef1 alpha Puro-T2A GFP vector (RRID:Addgene_111596) and lentivirus generated as previously described (42). Cells were plated in a six-well dish at 150,000 cells/well in 2 mL of media and infected with virus the next day with 10 μg/mL polybrene (TR-1003-G). Cells were harvested after 72 hours and analyzed as described above. Gene knockdown was measured by extracting RNA using the Zymo Quick-RNA MiniPrep Kit (R1054), performing cDNA synthesis using SuperScript III First Strand Synthesis Kit (18080051), and conducting qRT-PCR using Fast SYBR Green Master Mix (4385612) all according to the manufacturer's protocols.

Drug Treatments and Antibodies

C42B, LNCaP, VCaP, and PC3 cells were treated in their respective media with either DMSO, 10 μmol/L enzalutamide, or 100 nmol/L ARD for 14 days and refreshed every 5 days at minimum. Cells treated with CSS (Gibco) were maintained in phenol red-free media and refreshed every 7 days at minimum. Cells treated with the synthetic androgen R1881 (10 nmol/L) were refreshed every 3 days. Following 14 days of treatment, cells were harvested for flow cytometry and qRT-PCR (Supplementary Table S7), as described above, or Western blot analysis using anti-*AR* (D6F11), anti-MHCI (OriGene, Cat# AM33035PU-N, RRID:AB_3662758), or anti-Lamin B1 (Cell Signaling Technology, Cat# 15068, RRID:AB_2798695) antibodies. Gene expression of MHCI processing genes (normalized to *GAPDH*) was measured by qRT-PCR and compared with control. Drug-treated cells were stained with a fluorescent HLA-ABC antibody (17-9983-42) and analyzed using flow cytometry. Median fluorescence intensity (MFI) of cells stained with a fluorescent HLA-ABC antibody was measured by flow cytometry and compared with control to determine MHC fold change. MHCI expression of cells infected with sgRNAs targeting *GAL4* (nontargeting control), *AR*, *GRHL2*, *FOXA1*, or *B2M* was measured by flow cytometry and compared with *GAL4* to determine MHC fold change.

RNA Expression Analysis of Neoadjuvant Enzalutamide Patient Samples

Bulk RNA expression analysis of MHCI-related genes was performed on primary prostate cancer tissues before and after neoadjuvant enzalutamide treatment without ADT from the phase 2, prospective, single-arm DARANA study (ClinicalTrials.gov #NCT03297385) at the

Netherlands Cancer Institute Antoni van Leeuwenhoek Hospital. RNA-seq was performed as previously described (27). In brief, RNA from FFPE material was isolated from 2 to 10 sections of 10 μm using the AllPrep DNA/RNA FFPE Kit (Qiagen). cDNA was synthesized from 250 ng of RNA using SuperScript III Reverse Transcriptase (Invitrogen) with random hexamer primers. For RNA-seq, strand-specific libraries were generated with the TruSeq RNA Exome Kit (Illumina) and sequenced on a HiSeq 2500 (65-bp reads, single end). Sequencing data were aligned to hg38 using Hisat2 (RRID:SCR_015530; ref. 45), and the number of reads per gene was measured with HTSeq count (RRID:SCR_005514; ref. 46). For analyses, gene counts were normalized using DESeq2 (RRID:SCR_015687; ref. 47) and subsequently log transformed. Significance of expression level differences between pre- and posttreatment samples was determined using a Mann–Whitney U test. RNA-seq data from paired pre- and posttreatment prostate tumors from patients enrolled in a phase 2 clinical trial of 6 months of neoadjuvant ADT plus enzalutamide (ClinicalTrials.gov #NCT02430480) at the National Cancer Institute were downloaded from GEO (Study Accession: GSE183100; refs. 28, 48). Responding tumors with residual disease volumes less than 0.001 cm^3 were omitted from analysis ($n = 5$).

RNA-seq Analysis

RNA extraction was performed using the Zymo Quick-RNA MiniPrep Kit (R1054) and sent to the QB3 Genomics Sequencing Facility at UC Berkeley for library preparation and sequencing (RRID:SCR_022170). RNA-seq data were generated in FASTQ format. We quantified the gene-level expression using *kallisto* (49) and then used the abundance calls for downstream analysis. *DESeq2* (50) was used for differential gene expression analysis, including evaluating the effect size and statistical significance. Length-scaled transcripts per million (TPM) generated by *tximport* (51) were used for plotting gene expression values. For treatment × time interaction analysis, *P* values were evaluated using the likelihood ratio test implemented in DESeq2 to compare the full model [treatment (ENZA vs. DMSO), time (day 7, day 28, day 49, and day 91), and treatment × time interaction] with the reduced model (treatment and time without the interaction term). All statistical analyses were performed using R 4.2.0, and plots were generated using *ggplot2* (RRID:SCR_014601; https://cran.r-project.org/web/packages/ggplot2/citation.html).

ChIP-seq Analysis

ChIP-seq data for *AR* and H3K27ac were obtained from Hwang and colleagues (22). Briefly, Raw ChIP-seq data were downloaded from SRA (SRP222785). Reads with base quality scores more than 30 across all bases were aligned using bwa-mem v0.7.17 (RRID:SCR_022192; ref. 52) to build hg38. The aligned reads were deduplicated, and peaks were called using MACS2 v.2.2.5 (53) with a FDR threshold of 0.01. Peaks in ENCODE (RRID:SCR_015482) hg38 blacklist (ENCSR636HFF) were excluded, and only peaks that were enriched at least 10-fold more than background were kept for further analysis. The hg38 reference genome was segmented into 200-bp windows. The number of sequencing reads aligning to each window was determined and adjusted relative to the total number of mapped reads in the sample, yielding counts per million (CPM) values. Nonoverlapping unique ChIP-seq narrow peak regions were obtained from the samples analyzed, and CPM values for the 200-bp bins overlapping the ChIP-seq peaks were obtained. Further, the differential ChIP-seq analysis on the CPM values was performed using the Student *t* test.

ARE Identification, Sub-library Generation, and Screen Analysis

Genomic DNA was extracted from C42B cell lines using the ENZA tissue DNA kit (D3396-02), sheered using Covaris ME220 Focused Ultrasonicator (RRID:SCR_019818), and cleaned up using the MinElute Reaction Cleanup Kit (28204). Sample quality was assessed using a high-sensitivity DNA bioanalyzer kit (5067-4626) and sequenced on a NovaSeq S4 PE150 to reach 50× coverage per samples. Whole-genome sequence data were aligned to GRCh38 using the Burrows–Wheeler Aligner version 0.7.17 (52). The consensus sequence FASTA files were generated using bcftools algorithm version 1.9-213 (54). A list of AREs, including full, half-site, and lenient motifs (55), were downloaded as position site-specific matrix models from JASPAR database (RRID:SCR_003030; ref. 56). The Find Individual Motif Occurrences (FIMO) version 5.1 was employed to identify potential AREs upstream of MHC that may exist within FASTA files derived from the cell lines or using the Cistrome database (http://cistrome.org; ref. 57). Hits passing the FDR *q* value ≤ 0.05 were considered significant and prioritized by the highest FIMO occurrence score.

The Broad Institute sgRNA designer CRISPick was used to generate sgRNA sequences based on the location of the cut site (within the ARE sequence or a maximum of 3 bp outside), on-target cutting efficiency >0.2, and minimal off-target binding. In addition to ARE-targeting guides, 10% of the sub-library contained control guides targeting nonessential genes, positive control genes (*AR*, *GRHL2*, and *FOXA1*), negative control genes (*B2M*, *TAP1*, and *HLA-A*), and nontargeting guides. A 1-pmol guide pool was ordered from IDT with the addition of forward/reverse primer adapter sequences and a BSMBI cut site flanking the guide sequences. Cloning was performed using the Weissman lab protocol for cloning of pooled sgRNAs into lentiviral vectors with some modifications. In brief, libraries were amplified using HF Phusion enzymes (F-530S), purified using the MinElute Kit (28204), and cloned into the Lenti-CRISPR-V2 plasmid (Addgene, #52961). Ligation products were transformed with Stellar chemically competent cells (636736) and purified using Qiagen Maxi Prep Kit (12263). Guide distribution was validated by PCR using the Broad Institute's protocol for PCR of sgRNAs for Illumina sequencing using Ex Taq DNA Polymerase (RR001) and purified using SPRI select reagent (B23317) according to the Weissman lab protocol for Illumina Sequencing Sample Prep. Sample quality was assessed using a high-sensitivity DNA bioanalyzer kit (5067-4626) and sequenced on the MiSeq V3 150SR (RRID:SCR_016379) at the California Institute for Quantitative Biosciences at UC Berkeley. In evaluating element distribution, we took into account the 90% confidence interval of element abundance (i.e., the ratio between read counts of the 95th percentile most expressed element and that of the 5th percentile element). A 90% confidence interval less than 10 suggests a reasonably tight distribution with few missing elements.

Lentivirus was generated, and a FACS-based screen was performed as described above. In brief, C42B-dCas9 cells were infected with lentivirus containing an ARE-targeted sub-library at a 30% MOI for 3 days, selected with puromycin for 3 days, and allowed to recover for 24 hours. Cells were then fixed, stained with a HLA-ABC antibody, and sorted for 25% to 30% high and low MHC expression. DNA was extracted using the Zymo Quick-DNA FFPE Kit (56404) and amplified for 26 cycles using NEBNext Ultra II Q5 Master Mix (M0544S) and primers containing TruSeq indexes for NGS analysis. Libraries were purified using SPRI select reagent (B23317) according to the Weissman lab protocol for Illumina Sequencing Sample Prep. Sample quality was assessed using a high-sensitivity DNA bioanalyzer kit (5067-4626) and sequenced on a HiSeq 4000, SE50, at the UCSF Core Facility. Counts per target guide were calculated using MAGeCK (50) and normalized per sample by dividing by the total number of counts and multiplying with 1,000. Normalized counts were transformed by $\log_2$(normalized counts + 1). Differences between high and low MHCI groups were calculated at day 0 using the average of log-transformed counts across replicates. A *t* test was used to test for statistical significance per guide.

T-cell Isolation and Coculture

PBMCs were ordered from STEMCELL Technologies and T cells isolated using EasySep Human T Cell Isolation Kit (17951) according to the manufacture's protocol. Cells were resuspended in complete X VIVO media with 5% FBS, 10 mmol/L N-acetyl cysteine, 55 μmol/L ß-mercaptoethanol, and 50 IU/mL IL2. T cells were activated using Dynabeads Human T-Activator CD3/CD28 for T-Cell Expansion and Activation (11132D) and infected with lentivirus containing the *NY-ESO1* expression construct (Genecopoeia EX-Q0397-LV205) and 8 μg/mL polybrene 24 hours after activation. *NY-ESO1* expression was validated by flow cytometry 6 days postinfection. T cells were thawed the day prior to coculture in ATCC-modified RPMI media +10% FBS +5% penicillin/streptomycin + 1/10,000 IL2 + 5% human serum (H4522).

NY-ESO1 was expressed in C42B cells by infecting with lentivirus containing the *NY-ESO1* expression construct (Genecopoeia EX-Q0397-LV205) and 8 μg/mL polybrene and sorted twice for GFP expression. *NY-ESO1* expression was confirmed via Western blot (D1Q2U). For use in Incucyte experiments, C42B-NY-ESO1-expressing cells were infected with Nuclight Lentivirus Reagent (NLR; 4627) and sorted for RFP expression. For coculture experiments, C42B-NY-ESO1-NLR cells were treated with either DMSO, 10 μmol/L enzalutamide, 100 nmol/L ARD, or CSS for 14 days; drug treatment was refreshed at minimum every 5 days. Tumor cells were then harvested, washed, and replated in triplicate in a 96-well plate at either 2,500 or 10,000 cells per well, and T cells were added the following day. Cells were imaged and counted every 6 hours for 3 days using an Incucyte. For the indicated experiments, 5,000 U/mL of interferon gamma (I17001) was added 2 days prior to plating for coculture experiments and mouse anti-human HLA-ABC (311402) or IgG2a isotype control (400202) was added 2 hours prior to adding T cells.

Ar Knockdown TrampC1/PPSM Cells, Ar qPCR, and In Vitro Cell Growth Assessment

AR was deleted in TrampC1 or PPSM cells according to the protocol (58). sgRNA targeting the murine *Ar* gene (sgRNA 1: AATACTGAA TGACCGCCATC and sgRNA 4: GGGTGGAAAGTAATAGTCGA) and the mouse genome nontargeting *Ctrl* sgRNA (5′-GCACUACC AGAGCUAACUCA-3′) were obtained from Synthego. Cas9 recombinant protein was obtained from IDT. Following electroporation of the Cas9/sgRNA complex into 2×10^6 TrampC1 tumor cells, cells were plated in complete media and allowed to grow for 3 days. Cells were then subcloned, and 10 clones were analyzed for *Ar* expression by qPCR. Total RNA was extracted (RNeasy, Qiagen) and subjected to one-step RT-qPCR for *Ar* and *Sdha* (GoTaq one-step RT-qPCR) amplified in a QuantStudio 3 thermocycler (Applied Biosystems). Mouse qPCR primer sequences were as follows: mouse *Ar* (forward: 5′GGAGAACTACTCCGGACCTTAT3′; reverse: 5′GGGTGGAAAGT AATAGTCGATGG3′) and mouse *Sdha* (forward: 5′GAGATACGC ACCTGTTGCCAAG3′; reverse: 5′GGTAGACGTGATCTTTCTCA GGG3′). One clone with the lowest *Ar* mRNA expression was selected for further studies, referred to as TrampC1 *Ar*-KD. *In vitro* growth potential of TrampC1 *Ar*-KD cells was assessed by platting 5,000 cells in a 96-well plate, and confluency was measured using an Incucyte, with measurements every 2 hours for 30 hours.

MHCI Expression in TrampC1 and PPSM Cells by Flow Cytometry

To measure MHCI expression, 1×10^5 TrampC1 WT and TrampC1 *Ar*-KD or PPSM WT and PPSM *Ar*-KDc7 cells were plated in a six-well plate. Approximately 10 ng/mL of rIFNγ (BioLegend) was added. After 24 hours, cells were harvested and incubated on ice for 20 minutes with e506 fixable viability dye (eBioscience) and H-2Kb antibody (AF6-88.5, BioLegend, RRID:AB_2721683). Data were collected with a Fortessa Flow Cytometer (BD Biosciences) and analyzed using FlowJo software (Tree Star; RRID:SCR_008520).

In Vivo Mouse Studies

C57BL/6 (RRID:IMSR_JAX:000664), *Nur77*-GFP (RRID:IMSR_JAX:016617), and *Rag*2-KO (RRID:IMSR_JAX:008449) were purchased from the Jackson Laboratory. All animals were maintained under specific pathogen-free conditions in the Oregon Health & Science University animal facility. Eight-week-old males were used in all the experiments described. All cell lines were tested and confirmed to be *Mycoplasma*- and endotoxin-free using the MycoAlert Detection Kit (Lonza) and the Endosafe-PTS system (Charles River Laboratories). All animal experiments were approved by the Institutional Animal Care and Use Committee of OHSU. Animals were implanted with 1×10^6 TrampC1 WT, TrampC1 *Ar*-KDc6, PPSM WT, or PPSM *Ar*-KDc7 tumor cells passaged no more than three times after thawing on both hind flanks. Tumors were harvested and weighed 12 days postimplantation. Tumor-infiltrating lymphocytes (TIL) were isolated by dissection of tumor tissue into small fragments in a 50-cc conical tube followed by digestion at room temperature in a bacterial shaker at 180 rpm for 30 minutes in 1 mg/mL collagenase type IV (Worthington Biochemicals) and 20 mg/mL DNase (Roche) in PBS. Cells were then further disrupted with a 1-cc syringe plunger through a 70-μm nylon cell strainer (BD Biosciences) and filtered to obtain a single-cell suspension. TILs were incubated on ice for 20 minutes with e506 fixable viability dye (eBioscience), *Spas1* tetramer (peptide sequence STHVNHLHC, NIH tetramer core), and the following antibodies: CD8 (53-6.7, RRID:AB_11124344), TCRb (H57-597, RRID:AB_1272173), and CD44 (IM7, RRID:AB_494011). For intracellular cytokine staining, TILs were plated at 1×10^6 cells/well in 96-well plates and stimulated for 5 hours with PMA (80 nmol/L) and ionomycin (1.3 μmol/L) for restimulation, in the presence of brefeldin A (BFA). Cells were then stained for surface markers, fixed and permeabilized using the BD Cytofix/CytoPerm kit, and stained with IFNγ (XMG1.2, RRID:AB_466193) antibody. All the antibodies were purchased through BioLegend or eBioscience. Data were collected with a Fortessa Flow Cytometer (BD Biosciences) and analyzed using FlowJo software (Tree Star; RRID:SCR_008520). For long-term tumor growth assessment, tumors were measured using a caliper from day 8 until day 29.

Analysis of Previously Published Single-Cell RNA-seq Data

The recently published human PCa scRNA-seq dataset (30) was obtained from https://doi.org/10.17632/5nnw8xrh5m.1. We reanalyzed this dataset using the Seurat pipeline (RRID:SCR_016341; v4.1.0). The BBKNN algorithm (59) was employed to mitigate potential batch effects. Clustering and single-cell distribution were visualized using Uniform Manifold Approximation and Projection (UMAP) with the Leiden algorithm. Subsequently, cell clusters were annotated based on previously reported cell-type marker genes of human PCa (60) and the combined automatic annotation method CellTypist (61). *AR* activity was calculated using the VIPER analysis (62), an algorithm that employs the transcriptional gene regulatory network targeted by AR to infer its activity. Pathway activity of MHCI (3) or IFNγ was calculated using AUCell algorithm (v1.16.0). The preprocessed matrix of gene counts versus cells contained 40,270 cells from 19 individual biopsies from a total of 11 patients. Of patients published, our initial analysis included patients 1, 3, 5, 6, 7, 9, 10, 11, and 12. Patient 11 was not included in the published table but was included in the shared dataset. After clustering all cells, luminal cells were subset for further analysis. Patient 3 was excluded for subsequent analysis due to less than 1 luminal epithelial cell with ADT and/or upon recurrence.

Activity Analysis of WCDT Biopsy Samples

To measure *AR* regulon activity of each sample in the WCDT cohort, we used the VIPER R package (version 1.26.0; ref. 62). A log1p-transformed TPM gene expression matrix and a regulatory network were used as inputs for VIPER analysis. The *viper* function was employed to calculate *AR* activities. The regulatory network used in the VIPER analysis was the same as described above. To quantify the activity of the MHCI signature (*HLA-A*, *HLA-B*, *HLA-C*, *IRF2*, *TAP1*, *TAPBP*, and *B2M* genes) in each sample, we used the single-sample gene set enrichment analysis (ssGSEA; ref. 63) implemented in the GSVA (64) R package (version 1.44.5). The ssGSEA algorithm is a rank-based method to assess the expression levels of genes of a gene signature against all other genes in each sample within a given dataset. Log-transformed gene expression profiles and the MHCI signature were used as input to ssGSEA. FDR q values were used to determine statistical significance.

Master Regulator and GSEA Analysis

RNA-seq data of pembrolizumab-treated patient samples were used to evaluate differential transcription factor activities and to perform GSEA analysis (RRID:SCR_003199). Differential gene expression analysis between responders and nonresponders was first performed using DESeq2 (version 1.32.0; ref. 47). Gene expression differences were considered significant when the adjusted P value is <0.05. Transcription factor activity was inferred by msVIPER algorithms provided in the VIPER R package (version 1.26.0). The Wald test statistic results from DESeq2 output served as a gene list input data for the VIPER analysis. The transcriptional regulatory network used in this study was curated from four databases as previously described (65). GSEA version 3.0 (66) was used to identify gene sets that were significantly activated in pembrolizumab nonresponders compared with responders from the Hallmark database [version 7.4 of the Molecular Signatures Database (MSigDB; https://www.gsea-msigdb.org/gsea/msigdb/)]. The expression data normalized by variance-stabilizing transformation in DESeq2 were used as the input of GSEA, and the default metric Signal2Noise in GSEA was applied to calculate the differential expression with respect to nonresponders and responders. The gene sets were considered to be activated if their FDR q value was less than 0.05.

Statistical Analysis

Significance of expression level differences in primary prostate cancer pre- and posttreatment samples was determined using either a Mann–Whitney U test or a prespecified FDR significance level of 0.05 as indicated above. Unpaired t tests were used to determine the statistical significance for the column plots, denoted by asterisk (*). *, $P < 0.05$; **, $P < 0.01$; ***, $P < 0.001$. For mCRPC RNA-seq analysis, we calculated the correlation between two continuous variables using Pearson's correlation coefficients. The threshold of $P < 0.05$ indicates the significance of correlation.

Data Availability

RNA-seq data generated from the DARANA study are available in the European Genome-Phenome Archive (EGA) under the accession number EGAS00001006016. RNA-seq data from patient prostate tumors before and after 6 months of neoadjuvant ADT plus enzalutamide were downloaded from GEO (GSE183100). RNA-seq data and corresponding clinical annotations of tumor samples in WCDT cohort were downloaded from previously published studies (29). Single-cell RNA-seq data from patients with mHSPC were obtained from the authors (30). Newly generated RNA-seq data from 91 days of enzalutamide treatment in the C42B cells are available from GEO (GSE277299).

Authors' Disclosures

L.N. Chesner reports grants from Prostate Cancer Foundation and the Department of Defense during the conduct of the study. J.E. Hawley reports other support from GSK, Immunity Bio, Daichi Sankyo, and Seagen, grants from DOD, and other support from Prostate Cancer Foundation, AstraZeneca, BMS/Celgene, Barinthus, Crescendo Biologics, MacroGenics, PromiCell, Amgen, and Janssen outside the submitted work. M. Sjöström reports grants from the Prostate Cancer Foundation and the Swedish Cancer Society during the conduct of the study and personal fees from Astellas and Veracyte/Adelphi Targis outside the submitted work. X. Zhu reports grants from Conquer Cancer, the ASCO Foundation, Prostate Cancer Foundation, and the Department of Defense outside the submitted work. D. Kuzuoglu-Ozturk reports grants from the Department of Defense PCRP during the conduct of the study. D. Ruggero reports personal fees from eFFECTOR Therapeutics, Inc. outside the submitted work. C.G. Drake reports other support from Johnson and Johnson Innovative Medicine outside the submitted work. A.G. Sowalsky reports other support from Astellas during the conduct of the study. L. Fong reports grants and personal fees from AbbVie, Dendreon, and Roche/Genentech, grants from Amgen, BMS, Janssen, Merck, Nektar, and personal fees from Daiichi Sankyo, Sutro, and Innovent outside the submitted work. M.R. Cooperberg reports personal fees from Veracyte, Tempus, Bayer, Janssen, Merck, Pfizer, AstraZeneca, Astellas, ExactVu, Biomarker, and LynxDx outside the submitted work. A. Ashworth reports personal fees from Azkarra Therapeutics, Kytarro, Ovibio Corporation, Tango Therapeutics, Tiller tx, Cambridge Science Corporation, CytomX, Ambagon, Bluestar/ClearNote Health, Circle, Genentech, GLAdiator, HAP10, Earli, ORIC, Phoenix Molecular Designs, Trial Library, Yingli/280Bio, Next RNA, Novartis, and Prolynx outside the submitted work, as well as patents on the use of PARP inhibitors, held jointly with AstraZeneca, from which he has benefited financially (and may do so in the future). F.Y. Feng reports nonfinancial support from Artera, Astellas, Bayer, Blue Earth Diagnostics, Bristol Meyers Squibb, ClearNote, Myovant, Roivant, Sanofi, Serimmune, and Amgen and personal fees and nonfinancial support from Janssen, Point Biopharma, and Novartis outside the submitted work. A.E. Moran reports grants from the NIH/NCI, Prostate Cancer Foundation, Kuni Foundation, Collins Medical Trust, and UCSF during the conduct of the study, as well as a patent for WO 2023/049860 issued. No disclosures were reported by the other authors.

Authors' Contributions

L.N. Chesner: Conceptualization, data curation, formal analysis, supervision, funding acquisition, validation, investigation, visualization, methodology, writing–original draft, project administration, writing–review and editing. **F. Polesso:** Data curation, formal analysis, validation, investigation, visualization, methodology, writing–original draft, project administration, writing–review and editing. **J.N. Graff:** Resources, supervision. **J.E. Hawley:** Resources, supervision. **A.K. Smith:** Data curation, formal analysis, validation, investigation, visualization, methodology. **A. Lundberg:** Data curation, software, formal analysis, validation, investigation, visualization, methodology, writing–original draft. **R. Das:** Conceptualization, data curation, formal analysis, validation, investigation, methodology. **T. Shenoy:** Conceptualization, resources, data curation, formal analysis, validation, investigation, methodology, writing–original draft. **M. Sjöström:** Conceptualization, data curation, software, formal analysis, validation, investigation, visualization, methodology, writing–original draft, writing–review and editing. **F. Zhao:** Data curation, formal analysis, investigation, visualization, methodology. **Y.-M. Hu:** Data curation, formal analysis, investigation, visualization, methodology. **S. Linder:** Data curation, software, formal analysis, validation,

investigation, visualization, methodology, writing–original draft. **W.S. Chen:** Conceptualization, data curation, software, formal analysis, validation, investigation, visualization, methodology, writing–original draft. **R.M. Hawkins:** Data curation, formal analysis, writing–review and editing. **R. Shrestha:** Investigation. **X. Zhu:** Data curation, formal analysis, visualization. **A. Foye:** Data curation, validation, investigation. **H. Li:** Conceptualization, data curation, validation, investigation, methodology. **L.M. Kim:** Data curation, formal analysis, validation, investigation, visualization, methodology. **M. Bhalla:** Data curation, formal analysis, validation, investigation. **T. O'loughlin:** Data curation, formal analysis, validation, investigation, methodology. **D. Kuzuoglu-Ozturk:** Resources, methodology, writing–original draft. **J.T. Hua:** Conceptualization, resources, data curation, formal analysis, investigation, visualization, methodology. **M.L. Badura:** Data curation, formal analysis. **S. Wilkinson:** Data curation, formal analysis, investigation, writing–review and editing. **S.Y. Trostel:** Data curation, formal analysis, investigation. **A.M. Bergman:** Resources, supervision. **D. Ruggero:** Resources, supervision. **C.G. Drake:** Resources, supervision, writing–review and editing. **A.G. Sowalsky:** Resources, data curation, formal analysis, supervision, investigation, writing–review and editing. **L. Fong:** Supervision. **M.R. Cooperberg:** Supervision. **W. Zwart:** Resources, supervision. **X. Guan:** Resources, data curation, formal analysis, supervision, writing–review and editing. **A. Ashworth:** Conceptualization, resources, data curation, software, formal analysis, supervision, validation, investigation, visualization, methodology, writing–original draft, writing–review and editing. **Z. Xia:** Conceptualization, resources, data curation, software, formal analysis, supervision, validation, investigation, visualization, methodology, writing–original draft, writing–review and editing. **D.A. Quigley:** Conceptualization, resources, data curation, software, formal analysis, supervision, validation, investigation, methodology. **L.A. Gilbert:** Conceptualization, resources, data curation, software, formal analysis, supervision, funding acquisition, validation, investigation, visualization, methodology, writing–original draft, project administration, writing–review and editing. **F.Y. Feng:** Conceptualization, resources, data curation, software, formal analysis, supervision, funding acquisition, validation, investigation, visualization, methodology, writing–original draft, project administration, writing–review and editing. **A.E. Moran:** Conceptualization, resources, data curation, formal analysis, supervision, funding acquisition, validation, investigation, visualization, methodology, writing–original draft, project administration, writing–review and editing.

Acknowledgments

We would like to thank all the members of the Feng, Moran, and Gilbert labs for their helpful suggestions and technical advice, as well as Nicholas Larocque and Tina Yu for their administrative support. We thank Drs. Arul Chinnaiyan and Shaomeng Wang for the AR degrader. This study was supported in part by HDFCCC Laboratory for Cell Analysis Shared Resource Facility through the NIH grant (P30CA082103). L.N. Chesner is supported by the Prostate Cancer Foundation Young Investigator award and Department of Defense Early Investigator award (W81XWH2110046). J.E. Hawley is supported by grants from the Conquer Cancer Foundation (2019YIA to J.E. Hawley), the Prostate Cancer Foundation (2020YIA to J.E. Hawley), NCI SPORE P50 CA097186, and the NIH (T32CA203703 to J.E. Hawley, UL1TR001873 to J.E. Hawley). Z. Xia is supported by the Department of Defense Idea Development Award (W81XWH2110539) and NIH R01GM147365. Y.-M. Hu is supported by a postdoctoral fellowship of Portland Oral Health Research Training (PORT) T90 program (NIH T90 DE030859). M. Sjöström, R. Shrestha, and H. Li are supported by the Prostate Cancer Foundation Young Investigator award. X. Zhu is supported by the Prostate Cancer Foundation Young Investigator award and Department of Defense Physician Research Award through the Prostate Cancer Research Program (HT9425-24-1-0506). D. Kuzuoglu-Ozturk is supported by the UCSF Prostate Cancer Program Pilot Award. A.G. Sowalsky and S. Trostel are supported by The Intramural Research Program of the National Cancer Institute, National Institutes of Health. S. Wilkinson is supported by the Prostate Cancer Foundation Young Investigator award and Department of Defense Early Investigator award (W81XWH1910712) D. Ruggero is supported by NIH R35CA242986 and the American Cancer Society (RP-19–181–01-RMC). L. Fong is supported by a Prostate Cancer Foundation Challenge Award and NIH R35CA253175. D.A. Quigley is supported by funding from the Benioff Initiative for Prostate Cancer Research, the Prostate Cancer Foundation, NCI SPORE 1P50CA275741, and Department of Defense awards W81XWH-22-1-0833 and HT94252410252. L.A. Gilbert is funded by a Prostate Cancer Foundation Challenge Award (21CHAL06), a NIH New Innovator Award (DP2 CA239597), a Pew-Stewart Scholars for Cancer Research award, a CRUK/NIH Cancer Grand Challenges award (OT2CA278665; CGCATF-2021/100006), and the Goldberg-Benioff Endowed Professorship in Prostate Cancer Translational Biology. A.E. Moran is supported by a Prostate Cancer Foundation Young Investigator award, NCI SPORE P50 CA097186, and NIH/NCI R37CD263592. F.Y. Feng is supported by NIH/NCI 5R01CA227025 and Prostate Cancer Foundation Challenge Award. Additional funding was provided by a UCSF Benioff Initiative for Prostate Cancer Research award.

Note

Supplementary data for this article are available at Cancer Discovery Online (http://cancerdiscovery.aacrjournals.org/).

Received April 23, 2024; revised September 10, 2024; accepted December 3, 2024; published first December 5, 2024.

REFERENCES

1. Blades RA, Keating PJ, McWilliam LJ, George NJ, Stern PL. Loss of HLA class I expression in prostate cancer: implications for immunotherapy. Urology 1995;46:681–6.
2. Chen X, Lu Q, Zhou H, Liu J, Nadorp B, Lasry A, et al. A membrane-associated MHC-I inhibitory axis for cancer immune evasion. Cell 2023;186:3903–20.e21.
3. Bagaev A, Kotlov N, Nomie K, Svekolkin V, Gafurov A, Isaeva O, et al. Conserved pan-cancer microenvironment subtypes predict response to immunotherapy. Cancer Cell 2021;39:845–65.e7.
4. Lee JH, Shklovskaya E, Lim SY, Carlino MS, Menzies AM, Stewart A, et al. Transcriptional downregulation of MHC class I and melanoma de- differentiation in resistance to PD-1 inhibition. Nat Commun 2020;11:1897.
5. Sade-Feldman M, Jiao YJ, Chen JH, Rooney MS, Barzily-Rokni M, Eliane J-P, et al. Resistance to checkpoint blockade therapy through inactivation of antigen presentation. Nat Commun 2017;8:1136.
6. Zaretsky JM, Garcia-Diaz A, Shin DS, Escuin-Ordinas H, Hugo W, Hu-Lieskovan S, et al. Mutations associated with acquired resistance to PD-1 blockade in melanoma. N Engl J Med 2016;375:819–29.
7. Gao J, Shi LZ, Zhao H, Chen J, Xiong L, He Q, et al. Loss of IFN-γ pathway genes in tumor cells as a mechanism of resistance to anti-CTLA-4 therapy. Cell 2016;167:397–404.e9.
8. McGranahan N, Rosenthal R, Hiley CT, Rowan AJ, Watkins TBK, Wilson GA, et al. Allele-specific HLA loss and immune escape in lung cancer evolution. Cell 2017;171:1259–71.e11.
9. Goldman MJ, Craft B, Hastie M, Repečka K, McDade F, Kamath A, et al. Visualizing and interpreting cancer genomics data via the Xena platform. Nat Biotechnol 2020;38:675–8.
10. Bander NH, Yao D, Liu H, Chen YT, Steiner M, Zuccaro W, et al. MHC class I and II expression in prostate carcinoma and modulation by interferon-alpha and -gamma. Prostate 1997;33:233–9.

11. Mercader M, Bodner BK, Moser MT, Kwon PS, Park ES, Manecke RG, et al. T cell infiltration of the prostate induced by androgen withdrawal in patients with prostate cancer. Proc Natl Acad Sci U S A 2001;98:14565–70.
12. Obradovic AZ, Dallos MC, Zahurak ML, Partin AW, Schaeffer EM, Ross AE, et al. T-cell infiltration and adaptive Treg resistance in response to androgen deprivation with or without vaccination in localized prostate cancer. Clin Cancer Res 2020;26:3182–92.
13. Mercader M, Sengupta S, Bodner BK, Manecke RG, Cosar EF, Moser MT, et al. Early effects of pharmacological androgen deprivation in human prostate cancer. BJU Int 2007;99:60–7.
14. Guan X, Polesso F, Wang C, Sehrawat A, Hawkins RM, Murray SE, et al. Androgen receptor activity in T cells limits checkpoint blockade efficacy. Nature 2022;606:791–6.
15. Gilbert LA, Horlbeck MA, Adamson B, Villalta JE, Chen Y, Whitehead EH, et al. Genome-scale CRISPR-mediated control of gene repression and activation. Cell 2014;159:647–61.
16. Jin H-J, Zhao JC, Wu L, Kim J, Yu J. Cooperativity and equilibrium with FOXA1 define the androgen receptor transcriptional program. Nat Commun 2014;5:3972.
17. Paltoglou S, Das R, Townley SL, Hickey TE, Tarulli GA, Coutinho I, et al. Novel androgen receptor coregulator GRHL2 exerts both oncogenic and antimetastatic functions in prostate cancer. Cancer Res 2017;77:3417–30.
18. Zhao L, Han X, Lu J, McEachern D, Wang S. A highly potent PROTAC androgen receptor (AR) degrader ARD-61 effectively inhibits AR-positive breast cancer cell growth in vitro and tumor growth in vivo. Neoplasia 2020;22:522–32.
19. Kregel S, Wang C, Han X, Xiao L, Fernandez-Salas E, Bawa P, et al. Androgen receptor degraders overcome common resistance mechanisms developed during prostate cancer treatment. Neoplasia 2020; 22:111–9.
20. Bettoun DJ, Scafonas A, Rutledge SJ, Hodor P, Chen O, Gambone C, et al. Interaction between the androgen receptor and RNase L mediates a cross-talk between the interferon and androgen signaling pathways. J Biol Chem 2005;280:38898–901.
21. Baratchian M, Tiwari R, Khalighi S, Chakravarthy A, Yuan W, Berk M, et al. H3K9 methylation drives resistance to androgen receptor-antagonist therapy in prostate cancer. Proc Natl Acad Sci U S A 2022;119:e2114324119.
22. Hwang JH, Seo JH, Beshiri ML, Wankowicz S, Liu D, Cheung A, et al. CREB5 promotes resistance to androgen-receptor antagonists and androgen deprivation in prostate cancer. Cell Rep 2019;29:2355–70.e6.
23. Fassò M, Waitz R, Hou Y, Rim T, Greenberg NM, Shastri N, et al. SPAS-1 (stimulator of prostatic adenocarcinoma-specific T cells)/SH3GLB2: a prostate tumor antigen identified by CTLA-4 blockade. Proc Natl Acad Sci U S A 2008;105:3509–14.
24. Lu X, Horner JW, Paul E, Shang X, Troncoso P, Deng P, et al. Effective combinatorial immunotherapy for castration-resistant prostate cancer. Nature 2017;543:728–32.
25. Moran AE, Holzapfel KL, Xing Y, Cunningham NR, Maltzman JS, Punt J, et al. T cell receptor signal strength in Treg and iNKT cell development demonstrated by a novel fluorescent reporter mouse. J Exp Med 2011;208:1279–89.
26. Moran AE, Polesso F, Weinberg AD. Immunotherapy expands and maintains the function of high-affinity tumor-infiltrating CD8 T cells in situ. J Immunol 2016;197:2509–21.
27. Linder S, Hoogstraat M, Stelloo S, Eickhoff N, Schuurman K, de Barros H, et al. Drug-induced epigenomic plasticity reprograms circadian rhythm regulation to drive prostate cancer toward androgen independence. Cancer Discov 2022;12:2074–97.
28. Wilkinson S, Ye H, Karzai F, Harmon SA, Terrigino NT, VanderWeele DJ, et al. Nascent prostate cancer heterogeneity drives evolution and resistance to intense hormonal therapy. Eur Urol 2021;80:746–57.
29. Quigley DA, Dang HX, Zhao SG, Lloyd P, Aggarwal R, Alumkal JJ, et al. Genomic hallmarks and structural variation in metastatic prostate cancer. Cell 2018;174:758–69.e9.
30. Hawley JE, Obradovic AZ, Dallos MC, Lim EA, Runcie K, Ager CR, et al. Anti-PD-1 immunotherapy with androgen deprivation therapy induces robust immune infiltration in metastatic castration-sensitive prostate cancer. Cancer Cell 2023;41:1972–88.e5.
31. Obradovic A, Chowdhury N, Haake SM, Ager C, Wang V, Vlahos L, et al. Single-cell protein activity analysis identifies recurrence-associated renal tumor macrophages. Cell 2021;184:2988–3005.e16.
32. Ben-Batalla I, Vargas-Delgado ME, von Amsberg G, Janning M, Loges S. Influence of androgens on immunity to self and foreign: effects on immunity and cancer. Front Immunol 2020;11:1184.
33. Irelli A, Sirufo MM, D'Ugo C, Ginaldi L, De Martinis M. Sex and gender influences on cancer immunotherapy response. Biomedicines 2020;8:232.
34. Kwon H, Schafer JM, Song N-J, Kaneko S, Li A, Xiao T, et al. Androgen conspires with the CD8$^+$ T cell exhaustion program and contributes to sex bias in cancer. Sci Immunol 2022;7:eabq2630.
35. Gratzke C, Kwiatkowski M, De Giorgi U, Martins da Trindade K, De Santis M, Armstrong AJ, et al. KEYNOTE-991: pembrolizumab plus enzalutamide and androgen deprivation for metastatic hormone-sensitive prostate cancer. Future Oncol 2023;37:4079–87.
36. Zhang X, Cheng L, Gao C, Chen J, Liao S, Zheng Y, et al. Androgen signaling contributes to sex differences in cancer by inhibiting NF-κB activation in T cells and suppressing antitumor immunity. Cancer Res 2023;83:906–21.
37. Lakshmikanth T, Consiglio C, Sardh F, Forlin R, Wang J, Tan Z, et al. Immune system adaptation during gender-affirming testosterone treatment. Nature 2024;633:155–64.
38. Li F, Xing X, Jin Q, Wang XM, Dai P, Han M, et al. Sex differences orchestrated by androgens at single-cell resolution. Nature 2024 May;629:193–200.
39. Robert C, Lebbé C, Lesimple T, Lundström E, Nicolas V, Gavillet B, et al. Phase I study of androgen deprivation therapy in combination with anti-PD-1 in melanoma patients pretreated with anti-PD-1. Clin Cancer Res 2023;29:858–65.
40. Deng Y, Xia X, Zhao Y, Zhao Z, Martinez C, Yin W, et al. Glucocorticoid receptor regulates PD-L1 and MHC-I in pancreatic cancer cells to promote immune evasion and immunotherapy resistance. Nat Commun 2021;12:7041.
41. Arora VK, Schenkein E, Murali R, Subudhi SK, Wongvipat J, Balbas MD, et al. Glucocorticoid receptor confers resistance to antiandrogens by bypassing androgen receptor blockade. Cell 2013;155:1309–22.
42. Das R, Sjöström M, Shrestha R, Yogodzinski C, Egusa EA, Chesner LN, et al. An integrated functional and clinical genomics approach reveals genes driving aggressive metastatic prostate cancer. Nat Commun 2021;12:4601.
43. Horlbeck MA, Gilbert LA, Villalta JE, Adamson B, Pak RA, Chen Y, et al. Compact and highly active next-generation libraries for CRISPR-mediated gene repression and activation. Elife 2016;5:e19760.
44. Gilbert LA, Larson MH, Morsut L, Liu Z, Brar GA, Torres SE, et al. CRISPR-mediated modular RNA-guided regulation of transcription in eukaryotes. Cell 2013;154:442–51.
45. Kim D, Paggi JM, Park C, Bennett C, Salzberg SL. Graph-based genome alignment and genotyping with HISAT2 and HISAT-genotype. Nat Biotechnol 2019;37:907–15.
46. Anders S, Pyl PT, Huber W. HTSeq–a Python framework to work with high-throughput sequencing data. Bioinformatics 2015;31:166–9.
47. Love MI, Huber W, Anders S. Moderated estimation of fold change and dispersion for RNA-seq data with DESeq2. Genome Biol 2014;15:550.
48. Karzai F, Walker SM, Wilkinson S, Madan RA, Shih JH, Merino MJ, et al. Sequential prostate magnetic resonance imaging in newly diagnosed high-risk prostate cancer treated with neoadjuvant enzalutamide is predictive of therapeutic response. Clin Cancer Res 2021;27:429–37.
49. Bray NL, Pimentel H, Melsted P, Pachter L. Near-optimal probabilistic RNA-seq quantification. Nat Biotechnol 2016;34:525–7.
50. Li W, Xu H, Xiao T, Cong L, Love MI, Zhang F, et al. MAGeCK enables robust identification of essential genes from genome-scale CRISPR/Cas9 knockout screens. Genome Biol 2014;15:554.
51. Soneson C, Love MI, Robinson MD. Differential analyses for RNA-seq: transcript-level estimates improve gene-level inferences. F1000Res 2015;4:1521.

52. Li H, Durbin R. Fast and accurate short read alignment with Burrows-Wheeler transform. Bioinformatics 2009;25:1754–60.
53. Zhang Y, Liu T, Meyer CA, Eeckhoute J, Johnson DS, Bernstein BE, et al. Model-based analysis of ChIP-seq (MACS). Genome Biol 2008;9:R137.
54. Li H. A statistical framework for SNP calling, mutation discovery, association mapping and population genetical parameter estimation from sequencing data. Bioinformatics 2011;27:2987–93.
55. Wilson S, Qi J, Filipp FV. Refinement of the androgen response element based on ChIP-Seq in androgen-insensitive and androgen-responsive prostate cancer cell lines. Sci Rep 2016;6:32611.
56. Castro-Mondragon JA, Riudavets-Puig R, Rauluseviciute I, Lemma RB, Turchi L, Blanc-Mathieu R, et al. JASPAR 2022: the 9th release of the open-access database of transcription factor binding profiles. Nucleic Acids Res 2022;50:D165–73.
57. Grant CE, Bailey TL, Noble WS. FIMO: scanning for occurrences of a given motif. Bioinformatics 2011;27:1017–8.
58. Nüssing S, House IG, Kearney CJ, Chen AXY, Vervoort SJ, Beavis PA, et al. Efficient CRISPR/Cas9 gene editing in uncultured naive mouse T cells for in vivo studies. J Immunol 2020;204:2308–15.
59. Polański K, Young MD, Miao Z, Meyer KB, Teichmann SA, Park JE. BBKNN: fast batch alignment of single cell transcriptomes. Bioinformatics 2020;36:964–5.
60. Zhang T, Zhao F, Lin Y, Liu M, Zhou H, Cui F, et al. Integrated analysis of single-cell and bulk transcriptomics develops a robust neuroendocrine cell-intrinsic signature to predict prostate cancer progression. Theranostics 2024;14:1065–80.
61. Domínguez Conde C, Xu C, Jarvis LB, Rainbow DB, Wells SB, Gomes T, et al. Cross-tissue immune cell analysis reveals tissue-specific features in humans. Science 2022;376:eabl5197.
62. Alvarez MJ, Shen Y, Giorgi FM, Lachmann A, Ding BB, Ye BH, et al. Functional characterization of somatic mutations in cancer using network-based inference of protein activity. Nat Genet 2016;48:838–47.
63. Barbie DA, Tamayo P, Boehm JS, Kim SY, Moody SE, Dunn IF, et al. Systematic RNA interference reveals that oncogenic KRAS-driven cancers require TBK1. Nature 2009;462:108–12.
64. Hänzelmann S, Castelo R, Guinney J. GSVA: gene set variation analysis for microarray and RNA-Seq data. BMC Bioinformatics 2013;14:7.
65. Robertson AG, Shih J, Yau C, Gibb EA, Oba J, Mungall KL, et al. Integrative analysis identifies four molecular and clinical subsets in uveal melanoma. Cancer Cell 2017;32:204–20.e15.
66. Subramanian A, Tamayo P, Mootha VK, Mukherjee S, Ebert BL, Gillette MA, et al. Gene set enrichment analysis: a knowledge-based approach for interpreting genome-wide expression profiles. Proc Natl Acad Sci U S A 2005;102:15545–50.